

A Large-Eddy-Simulation Study of Combustion Dynamics of Bluff-Body Stabilized Flames

Hua-Guang Li, Prashant Khare , Hong-Gye Sung, and Vigor Yang

School of Aerospace Engineering, Georgia Institute of Technology, Atlanta, Georgia, USA

ABSTRACT

A comprehensive numerical study is conducted to explore the dynamic behaviors of a flame stabilized by a triangular bluff body in a straight chamber. The formulation accommodates the complete set of conservation equations with turbulence closure achieved by a large eddy simulation (LES) technique. A G-equation-based level-set flamelet approach is employed to model the interactions between premixed combustion and turbulence. Both non-reacting and reacting flows are treated, with special attention given to the effect of inlet boundary conditions on the flame evolution. The flow around the bluff body consists of boundary layers, separated shear layers, a recirculation zone and a wake. Their mutual coupling, as well as interactions with acoustic motion and flame oscillation are analyzed in detail. The physical processes responsible for driving combustion instabilities and the mechanism of energy transfer from chemical reactions in the flame zone to acoustic oscillations in the bulk of the chamber are investigated systematically. Intensive resonance is found to occur between shear-layer instabilities and chamber acoustic waves, when the acoustically reflecting inlet boundary condition is enforced. The resulting complex interplay among acoustic motion, vortex shedding, and unsteady heat release forms a feedback loop and excites combustion instabilities with large flow oscillations.

ARTICLE HISTORY

Received 8 July 2015
Revised 12 November 2015
Accepted 22 December 2015



KEYWORDS

Bluff-body; Combustion instability; Large eddy simulation (LES); Premixed flames

Introduction

Bluff-body stabilized flames are widely used in various combustion devices where the flow speed is much higher than the flame speed. A bluff body is usually placed in the chamber with its axis often perpendicular to the flow direction. Immediately downstream of the bluff body, burned gases are entrained in the recirculation zone, which provides a continuous ignition source to anchor and stabilize the flame. The bluff body is thus referred to as a flame holder or a flame stabilizer.

The flow around a bluff body consists of a boundary layer, a separated shear layer, a recirculation zone, and a wake (Cimbala, 1984; Prasad and Williamson, 1997). For Reynolds numbers below 2×10^5 , the dynamics of the flow field can be characterized by the behaviors of the shear layer and the wake, without major contributions from the boundary layer (Shanbhogue et al., 2009a). The separated shear layer forms the boundary of the recirculation zone behind the bluff body. The associated flow instability is of the

CONTACT Vigor Yang  vigor@gatech.edu  School of Aerospace Engineering, Georgia Institute of Technology, 270 Ferst Drive NW, Atlanta, GA 30332, USA.

Color versions of one or more of the figures in the article can be found online at www.tandfonline.com/gcst.

Kelvin–Helmholtz (KH) type. The instability associated with the wake region, commonly known as the Bénard/von Karman (BVK) instability, leads to periodic vortex shedding from opposite sides of the bluff body and the creation of a sinuous wake (Cimbala, 1984).

Chemically reacting flows differ considerably from their non-reacting counterparts due to the effects of heat release and volume dilatation. The BVK vortex shedding is suppressed by the heat release and, in the case of a triangular bluff body, a pair of symmetric stationary vortices forms at the two opposite edges (Fureby, 2000). For cases with large heat release, i.e., the temperature ratio of the burned to the unburned gases T_b/T_u (or ρ_u/ρ_b) is large, the BVK vortex shedding is absent. The wake is relatively flat compared to non-reacting flows, and the flame dynamics are dominated by the KH instability (Erickson et al., 2006). The transition from asymmetric to symmetric vortex shedding takes place between density ratios of 1.7–3.4. Sinusoidal shedding, however, can occasionally occur for higher density ratios, the arrival rate and duration of which decreases with increasing density ratio (Cocks et al., 2015; Emerson et al., 2012).

Extensive efforts have been made to study the combustion dynamics of bluff-body stabilized flames (Fujii and Eguchi, 1981; Sanquer et al., 1998; Shanbhogue et al., 2007; Shcherbik et al., 2009; Shin et al., 2011; Sivakumar and Chakravarthy, 2008; Sjunnesson et al., 1991a, 1991b, 1992; Zukoski, 1997; Zukoski and Marble, 1956). Zukoski experimentally explored the time-averaged characteristics and flammability limits of bluff-body stabilized flames under steady-state conditions (Zukoski, 1997; Zukoski and Marble, 1956). Sjunnesson et al. (1991a, 1991b, 1992) studied turbulent flow characteristics of v-gutter stabilized premixed propane/air flames. Non-intrusive measurements of velocity, temperature, and species concentrations were conducted using laser Doppler velocimetry (LDV), 2- λ coherent anti-Stokes Raman spectroscopy (CARS), and gas analysis, respectively. Density gradients and visible light emissions from the combustion phenomenon were acquired by means of Schlieren imaging and high-speed photography. Sanquer et al. (1998) performed detailed experiments on bluff-body stabilized premixed combustion. The characteristic alternate vortex shedding pattern was not observed in reacting flows, in contrast to the corresponding non-reacting flows; instead, longitudinal acoustic oscillations associated with the symmetric flapping of the flame front anchored at the flameholder edges were noticed. Fujii and Eguchi (1981) experimentally compared the turbulence properties of reacting and non-reacting bluff-body stabilized flows. The turbulence intensity and vortex shedding were found to be suppressed by combustion.

Shcherbik et al. (2009) employed optical diagnostics to study the dynamics of v-gutter stabilized flames with Jet-A fuel. Two intense longitudinal acoustic instabilities were identified using pressure sensors and a high-speed camera. The BVK instability was also observed in the form of a snake-like flame shape by means of high-speed imaging. Shanbhogue et al. (2007) experimentally investigated the effect of acoustic excitation on bluff-body stabilized flames. The interactions between the vorticity field and flame evolution were quantified for the downstream region. The vortical disturbances were found to be strongly influenced by the effects of enhanced diffusion in the heat-release zone, volume dilation, and baroclinic torque. Shin et al. (2011) investigated the response of bluff-body stabilized flames to harmonic oscillations. The excitation of hydrodynamic flow instabilities by acoustic waves, as well as the flame response to these instabilities, was addressed. Sivakumar and Chakravarthy (2008) conducted experiments on bluff-body stabilized methane/air flames

to investigate blow-off limits and acoustic characteristics by means of pressure measurements and flame visualization using CH^* chemiluminescence.

Analytical study of the behaviors of bluff-body stabilized flames commenced in the 1940s. Tsien (1951) investigated flame spreading characteristics under steady-state conditions using an integral method. The method was later extended by Marble and Candel (1979) to treat the flame response to longitudinal acoustic excitations from both the upstream and downstream regions. A similar technique was employed by Yang and Culick (1986) to investigate combustion instabilities in a ramjet engine with a dump combustor. The effect of the recirculating flow behind the flame holder was taken into account.

In recent years, numerical simulations using Reynolds averaged Navier Stokes (RANS) equations coupled with different types of combustion models have been widely employed to predict time-averaged flow distributions (Poinso and Veynante, 2005). The time-mean properties, however, cannot explain the inherent unsteady and dynamic nature of the flame stabilized by a bluff body (Shcherbik et al., 2009). Increases in computing power and advances in numerical methodologies have made possible the use of large eddy simulation (LES) techniques (Grinstein et al., 2007; Sagaut, 2002) to perform three-dimensional (3D) time-accurate calculations of flows involving turbulent combustion. Fureby and Möller (1995) employed LES to examine both non-reacting and reacting flows around a triangular bluff body under a variety of operating conditions. Typical unsteady flow structures were resolved. Baudoin et al. (2009) and Fureby (2006) further compared the predictive capabilities of several combustion models applied to bluff-body stabilized flames. They considered theoretical links between different models in terms of the flame speed and geometry. Giacomazzi et al. (2004) studied turbulence chemistry interactions in a premixed bluff-body stabilized flame using LES and eddy-dissipation concept models. Both 2D and 3D non-reacting and reacting flows were treated. Results revealed that 3D vortical structures periodically shorten the wake and entrain fresh reactants into the hot recirculation zone. It was pointed out that the periodic boundary conditions in the spanwise direction employed in the 2D case do not capture the impact of sidewalls, including the shortening of the recirculation zone, the flow acceleration downstream, and the wall heat transfer.

In spite of the rich literature on numerical investigations of v-gutter stabilized turbulent premixed flames (Baudoin et al., 2009; Briones et al., 2011; Cocks et al., 2015; Engdar et al., 2003, 2004; Erickson and Soteriou, 2011; Erickson et al., 2006; Fureby, 1996, 2000, 2007a, 2007b; Fureby and Löfström, 1994; Fureby and Möller, 1995; Ge et al., 2007; Ghirelli, 2011; Giacomazzi et al., 2004; Jones et al., 2015; Kim and Pope, 2014; Lee and Cant, 2014; Lin and Holder, 2010; Manickam et al., 2012; Moreau, 2009; Nilsson and Bai, 2000; Olovsson, 1992; Park and Ko, 2011; Porumbel and Menon, 2006; Ryden et al., 1993; Salvador et al., 2013; Sivakumar and Babu, 2008; Sundaram and Babu, 2013; Zhou et al., 2008), very few studies attempted to quantitatively identify the mechanisms dictating the interactions between the flame dynamics, shear layers, heat release, and acoustic waves. Most existing studies were concentrated on numerical code validation against measurements of velocity and temperature under stationary conditions. One notable exception is the study by Sundaram and Babu (2013), which dealt with acoustic motion and its interaction with flame dynamics using LES. This work was based on a commercial code, FLUENT, and presented no model validation for the flowfield. The evolution of flow and

flame structures was not discussed either. Recently, Cocks et al. (2015) conducted careful studies to investigate the effect of numerical error on the predictive capabilities of LES-based numerical codes for v-gutter stabilized premixed flames. They suggested that in addition to sub-grid scale models, numerical error can have a notable influence on the resulting flow field.

Understanding combustion instability is of great importance in improving combustor designs (Lieuwen and Yang, 2005), developing control strategies (Fung and Yang, 1992; Fung et al., 1991) and reducing harmful emissions (Lieuwen and Yang, 2013). Combustion instabilities exhibited by a bluff-body stabilized flame are affected by such factors as the equivalence ratio of the reactants, geometry and position of the flame holder, flow blockage, density ratio (Emerson et al., 2012), acoustic forcing (Shanbhogue et al., 2009b), and heat-release distribution. The focus of the present work is to comprehensively study the interactions among the flow evolution, acoustic excitation, and combustion response occurring in a premixed propane/air flame stabilized by a confined triangular bluff body. The model employs LES techniques and a level-set flamelet approach to explore the overall combustion dynamics. Underlying mechanisms and key parameters dictating the flow and combustion behaviors are identified and characterized systematically. The study also includes a thorough investigation of the effect of acoustically reflecting and non-reflecting inlets on combustion dynamics, which remains an open issue in the literature for v-gutter stabilized premixed flames.

Theoretical formulation

The present study is based on the theoretical formulation and computational framework developed by Huang et al. (2003). The 3D formulation consists of the Favre-filtered conservation equations of mass, momentum, and energy. They are obtained by filtering the small scales from the resolved scales over a well-defined set of spatial and temporal domains. The equations can be conveniently expressed in the following Cartesian tensor form:

$$\frac{\partial \bar{\rho}}{\partial t} + \frac{\partial \bar{\rho} \tilde{u}_i}{\partial x_i} = 0 \quad (1)$$

$$\frac{\partial \bar{\rho} \tilde{u}_i}{\partial t} + \frac{\partial (\bar{\rho} \tilde{u}_i \tilde{u}_j + \bar{p} \delta_{ij})}{\partial x_j} = \frac{\partial (\tilde{\tau}_{ij} - \tau_{ij}^{sgs})}{\partial x_j} \quad (2)$$

$$\frac{\partial \bar{\rho} \tilde{E}}{\partial t} + \frac{\partial ((\bar{\rho} \tilde{E} + \bar{p}) \tilde{u}_i)}{\partial x_i} = \frac{\partial}{\partial x_i} (\tilde{u}_j \tilde{\tau}_{ij} + \lambda \frac{\partial \tilde{T}}{\partial x_i} - H_i^{sgs} + \sigma_i^{sgs}) \quad (3)$$

where overbars and tildes denote resolved-scale and Favre-averaged resolved-scale variables, respectively. τ_{ij} is the viscous stress tensor. A detailed derivation of the filtered equations can be found in Oefelein and Yang (1996). The unresolved *sgs* terms in Eqs. (2) and (3), including the stress τ_{ij}^{sgs} , the energy flux H_i^{sgs} , and the viscous work σ_i^{sgs} , are given as:

$$\tau_{ij}^{sgs} = (\overline{\rho u_i u_j} - \bar{\rho} \tilde{u}_i \tilde{u}_j) \quad (4)$$

$$H_i^{sgs} = (\overline{\rho E u_i} - \tilde{\rho} \tilde{E} \tilde{u}_i) + (\overline{p u_i} - \tilde{p} \tilde{u}_i) \quad (5)$$

$$\sigma_i^{sgs} = (\overline{u_j \tau_{ij}} - \tilde{u}_j \tilde{\tau}_{ij}) \quad (6)$$

The algebraic version of the Smagorinsky model suggested by Erlebacher et al. (1992) is used to close the *sgs* shear stress τ_{ij}^{sgs} . Flow inhomogeneities near the wall are treated using the Van Driest damping function. The *sgs* viscous work, σ_i^{sgs} , is neglected due to its small contribution to the total energy equation. Further details about the closure models can be found in Huang et al. (2003).

Turbulent premixed combustion involves a wide range of length and time scales associated with flow motions and chemical reactions. The turbulent Reynolds number, Re , and the Karlovitz number, Ka , are often used to characterize turbulence/chemistry interactions:

$$Re = v' l / (S_L l_F) \quad (7)$$

$$Ka = t_F / t_\eta \approx l_F^2 / \eta^2 \quad (8)$$

where v' is the turbulent velocity fluctuation, l the turbulent integral length scale, S_L and l_F the flame speed and thickness, respectively, t_F and t_η the flame and the Kolmogorov time scales, respectively, and η is the Kolmogorov length scale. Based on the relative importance of the two non-dimensional numbers, turbulent premixed combustion can be classified into four regimes (Peters, 2000). Corrugated flamelets occur when $Re > 1$, $v'/S_L > 1$, and $Ka < 1$. In this regime, turbulent velocity fluctuations are large enough to allow eddies to corrugate the flame front. The smallest eddies of size η , however, are still larger than the laminar flame thickness l_F , and thus exert limited effects on the flame structure. In all of the cases studied in the present work, the Karlovitz number is less than 1 and the flamelet assumption holds. The premixed turbulent flame can be treated as a collection of thin reaction diffusion layers, commonly referred to as flamelets (Herrmann, 2000). These flamelets are embedded in an otherwise chemically equilibrated turbulent flow field. The filtered mean flame is regarded as the average of different laminar flamelets, which randomly fluctuate around the mean flame position under the effects of unresolved small-scale turbulence. The mean location of flamelets is obtained by solving a level-set transport equation.

The turbulent premixed flame is modeled using a G-equation approach, which attempts to describe the premixed turbulent combustion from a geometrical point of view. The flame front is represented by an arbitrary iso-surface G_0 in a scalar field of G , whose evolution is formulated using the so-called G-equation. The theoretical formulation and implementation details of the G-equation approach and the closure models used in the present study can be found elsewhere (Huang et al., 2003; Peters, 2000).

Conservation of the Favre-filtered G variable \tilde{G} , defined as a distance normal to the flame front, is enforced by a re-initialization process. Since the discretized level-set equation contains spatial gradients of \tilde{G} , dependency on values of $\tilde{G} \neq \tilde{G}_0$ near the flame surface is introduced. To maintain the numerical accuracy, $|\nabla \tilde{G}| = 1$ is enforced (Herrmann, 2000) using the methodology developed by Sussman et al. (1994).

A presumed probability density function (PDF) method is used along with a resolved flamelet structure to obtain the mean chemical composition of the premixed turbulent flame. The probability of finding the instantaneous flame front is presumed using a Gaussian distribution (Peters, 2000). Details of the presumed PDF approach can be found in Huang et al. (2003).

The inner structure of the premixed flame is calculated separately by taking into account finite-rate chemistry, using the GRI-MECH 3.0 reaction mechanism. A library is established for a propane/air mixture with an equivalence ratio of 0.6 at 1 atm by solving a system of transport equations for the temperature and species-concentration fields for a freely propagating planar flame (Nilsson and Bai, 2000). The coupling of the flow equations and the flamelet library is treated following the approach used by Herrmann (2000). The thermophysical variables extracted from the flamelet library are the ratio of specific heats, the gas constant R , and the enthalpy of formation of the mixture. Heat release data is also obtained from the flamelet library.

Numerical method

The governing equations and boundary conditions are solved numerically by means of a density-based, finite-volume methodology. The spatial discretization employs a second-order, central-differencing scheme in generalized coordinates. Fourth-order matrix dissipation with a total-variation-diminishing switch is employed to ensure computational stability and to prevent numerical oscillations in regions with steep gradients (Huang et al., 2003). Temporal discretization is obtained using a four-step Runge–Kutta integration scheme. Multi-block domain decomposition is used to facilitate the implementation of parallel computation with message passing interfaces at the domain boundaries. The theoretical and numerical framework described above has been validated against a wide variety of problems, including gas-turbine injectors (Wang and Yang, 2005; Wang et al., 2007) and simulated rocket motor flow dynamics (Apte and Yang, 2003).

Configuration and boundary conditions

Figure 1 shows the flame-holder geometry considered in the present study, simulating the experiments reported by Sjunnesson et al. (1991b). The test section consists of a 3D triangular bluff body placed in a channel with a square cross section (0.12×0.12 m). The channel length is 1.0 m. The dimension (H) of the triangular body is 4 cm on each side. In the spanwise z direction, the bluff body extends from one side of the channel to the other.

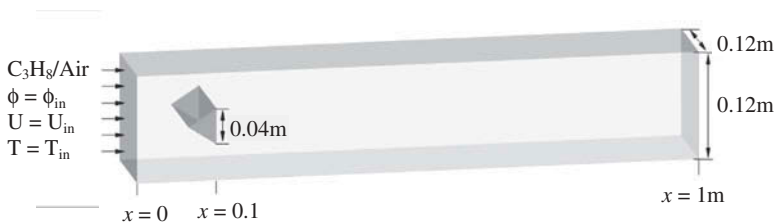


Figure 1. Schematic of triangular bluff-body flame holder in rectangular channel.

Table 1. Boundary and input conditions.

Cases	Flow	u_{in} (m/s)	T_m (K)	ϕ_{in}	Re	Acoustic boundary at inlet
1	Non-reacting	17	288	0	45,000	Reflecting
2	Non-reacting	36	600	0.6	28,000	Reflecting
3	Reacting	36	600	0.6	28,000	Reflecting
4	Reacting	36	600	0.6	28,000	Non-reflecting

A premixed propane/air mixture is delivered to the channel. The plane $x = 0$ is located at the flow inlet boundary.

Table 1 lists the flow conditions for the four cases treated herein, including both non-reacting and reacting flows. The reacting flows are modeled with both acoustically reflecting and non-reflecting boundary conditions at the inlet. The equivalence ratio of the fuel/air mixture remains fixed at 0.6. The specific boundary conditions are specified based on linear acoustic theories.

Figure 2 shows a schematic of the acoustic field, consisting of two waves traveling upstream and downstream. They can be described as:

$$p'_a = (P^+ e^{ikx} + P^- e^{-ikx})e^{-i\Omega t} \tag{9}$$

$$u'_a = \frac{1}{\rho \bar{a}} (P^+ e^{ikx} - P^- e^{-ikx})e^{-i\Omega t} \tag{10}$$

where P^+ and P^- represent the amplitudes of the two traveling waves, respectively. The complex frequency Ω is given by:

$$\Omega = \omega + i\alpha \tag{11}$$

where ω is the radian frequency and α the damping coefficient. The wave number k is defined as:

$$k = \Omega/\bar{a} \tag{12}$$

The reflecting boundary condition at the inlet corresponds to an acoustically rigid boundary, where the local acoustic velocity vanishes.

$$u'_a = 0 \tag{13}$$

The inlet velocity thus becomes the sum of its time-mean and turbulent quantities.

$$\tilde{u} = u_0 + u'_t \tag{14}$$

The isentropic flow assumption is assumed to hold at the inlet boundary for both reflecting and non-reflecting flows to obtain the temperature at the inlet.

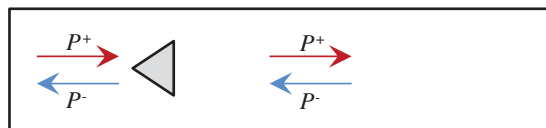


Figure 2. Acoustic field with two traveling waves in the chamber.

$$\tilde{T} = T_{\infty}(\bar{p}/p_{\infty})^{\frac{\gamma}{\gamma-1}} \quad (15)$$

The pressure is extrapolated from the interior points according to the characteristic relationship. The non-reflecting boundary conditions, wherein the acoustic waves can pass through the boundary without being reflected, can be represented by:

$$P^+ = 0 \text{ and } u'_a = -\frac{p'_a}{\rho a} \quad (16)$$

The velocity at the inlet consists of contributions from the time-mean, acoustic, and turbulent fields as follows (Huang et al., 2006):

$$\tilde{u} = u_0 + u'_a + u'_t \quad (17)$$

The non-reflecting inlet boundary condition used in the current study is close to the experimental conditions of Sjunnesson et al. (1991b), where the inlet was acoustically isolated by a perforated plate. Non-slip adiabatic boundary conditions are enforced on the walls. For the outlet boundary, pressure is set to one atmosphere and other primitive variables are obtained from the upstream region. Periodic boundary conditions are applied at the spanwise boundaries.

Results and discussion

Time-mean flowfield

The theoretical and numerical framework described in the preceding sections is applied to investigate the turbulent premixed combustion of propane and air over a triangular bluff body, as illustrated in Figure 1. Nine million grid points are used to discretize the whole domain, with 100 grid points employed each in the spanwise (z) and normal (y) directions. In order to resolve detailed flow structures adequately, the axial (x) and normal grid points are clustered near the bluff body and in the shear layers. The spanwise grid is uniformly distributed. The Kolmogorov and Taylor length scales for $Re = 28,000$ ($T = 600$ K) are 8.1 and 430 μm , respectively. The corresponding time scales are 3.8 and 14 μs , respectively. The CFL number employed in the current study is 0.7 and the smallest grid size is 0.1 mm. The spatial resolution is chosen based on the inlet Reynolds numbers, such that the largest grid size falls in the inertial sub-range of the turbulent energy spectrum. In comparison, Baudoin et al. (2009) used 0.4 million grid points, with the characteristic spacing of 1 mm. Since no grid resolution criteria for LES of reacting flows exist in the literature (Cocks et al., 2015), the computational grid used in the present work is conservative.

The analysis was validated against the experimental measurements reported by Sjunnesson et al. (1991b) for both non-reacting (case 1) and reacting flows (cases 3 and 4). Calculations were performed for an extended period of time until statistically meaningful data were obtained. The mean flowfield was determined by averaging over eight flow-through cycles (222 ms), after the initial transients were convected out of the flow domain over the first five cycles (138 ms). Figure 3 shows the vertical distributions of the predicted and measured axial velocities for the non-reacting case at three different streamwise locations ($x/H = 8.5, 11.5,$ and 16.5) at the mid-section in the spanwise direction. The velocities are normalized with the inlet velocity. Both the mean and root mean square (rms) values show excellent agreement. The

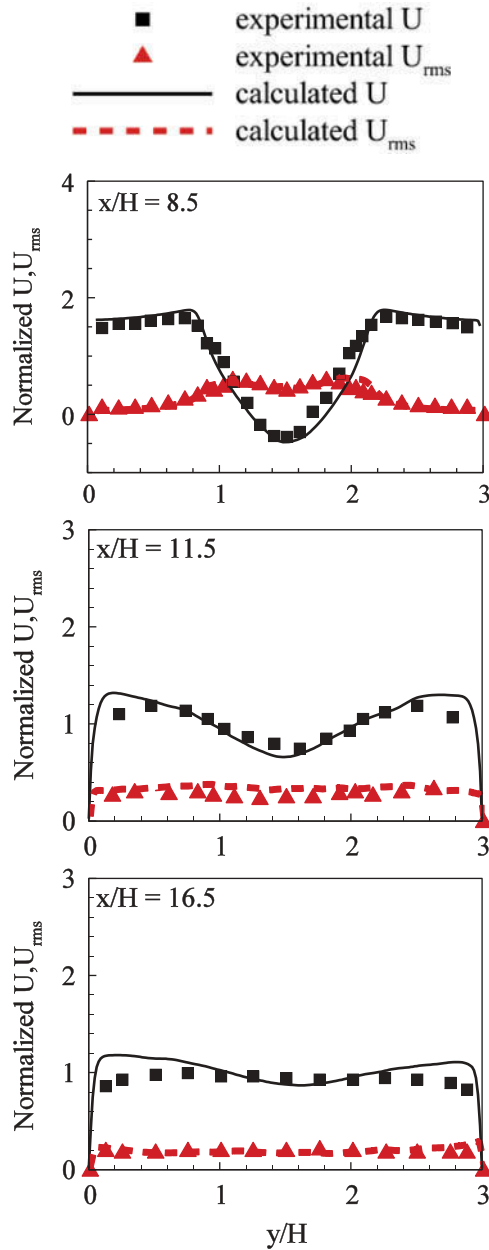


Figure 3. Vertical distributions of predicted and measured (Sjunnesson et al., 1991b) mean and rms values of streamwise velocity normalized by the mean velocity at the inlet boundary at different streamwise locations ($x/H = 8.5, 11.5, 16.5$) for non-reacting flow.

effect of the wake decreases in the downstream region, rendering the velocity profiles relatively flat.

Figure 4 shows the mean axial velocity profiles at different streamwise locations for the reacting flow. Both of the cases with the acoustically reflecting and non-reflecting inlet

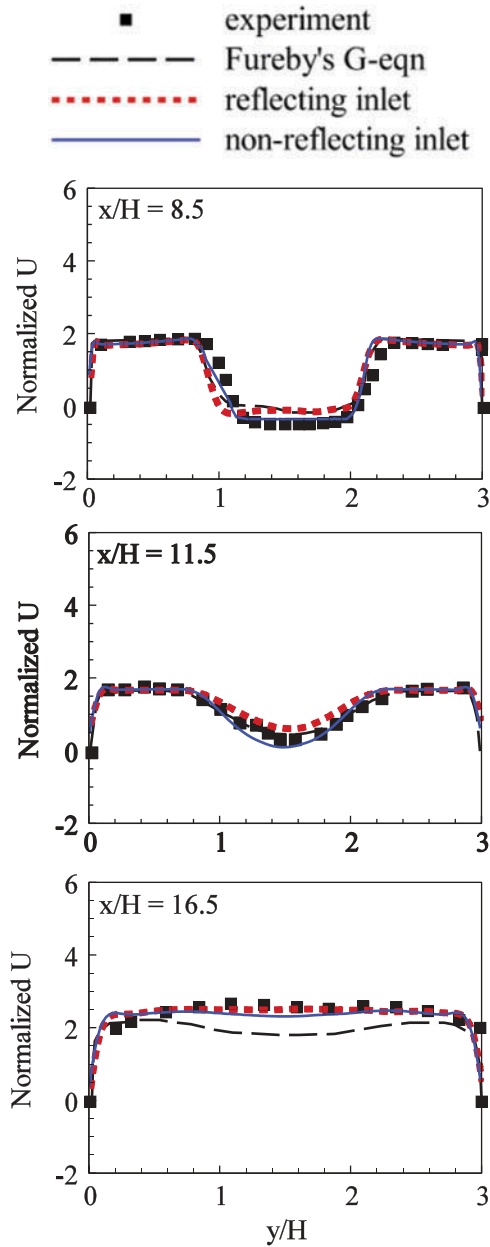


Figure 4. Vertical distributions of predicted and measured (Sjunnesson et al., 1991b) mean values of axial velocity normalized by the mean velocity at the inlet boundary at different streamwise locations ($x/H = 8.5, 11.5, 16.5$) for reacting flow.

boundary conditions are compared with experimental data (Sjunnesson et al., 1991b). Also included are the LES results of Fureby and co-workers, who used a flamelet-based approach (Baudoin et al., 2009). The velocity in the downstream region is noticeably

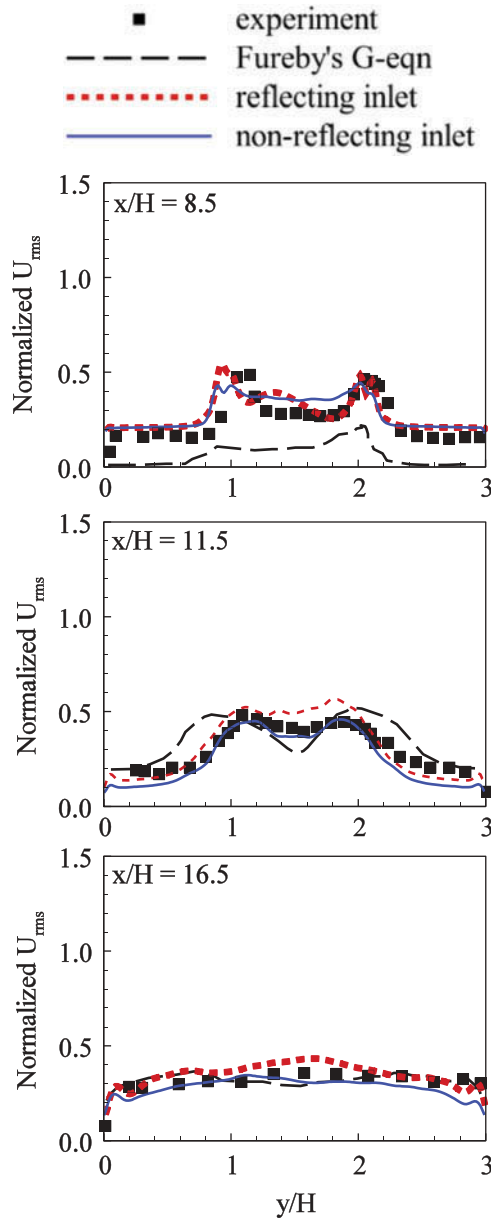


Figure 5. Vertical distributions of predicted and measured (Sjunnesson et al., 1991b) rms values of axial velocity normalized by the mean velocity at the inlet boundary at different streamwise locations ($x/H = 8.5, 11.5, 16.5$) for reacting flow.

higher than its non-reacting counterpart, due to the effect of heat release. Figure 5 shows the comparison of predicted and measured rms velocity profiles.

The results for the mean temperature profiles are given in Figure 6, where T_{ad} denotes the adiabatic flame temperature. The peak temperature decreases with downstream locations because of thermal diffusion in the vertical direction. The present work provides a marked improvement in predicting flow characteristics over the previous analysis reported

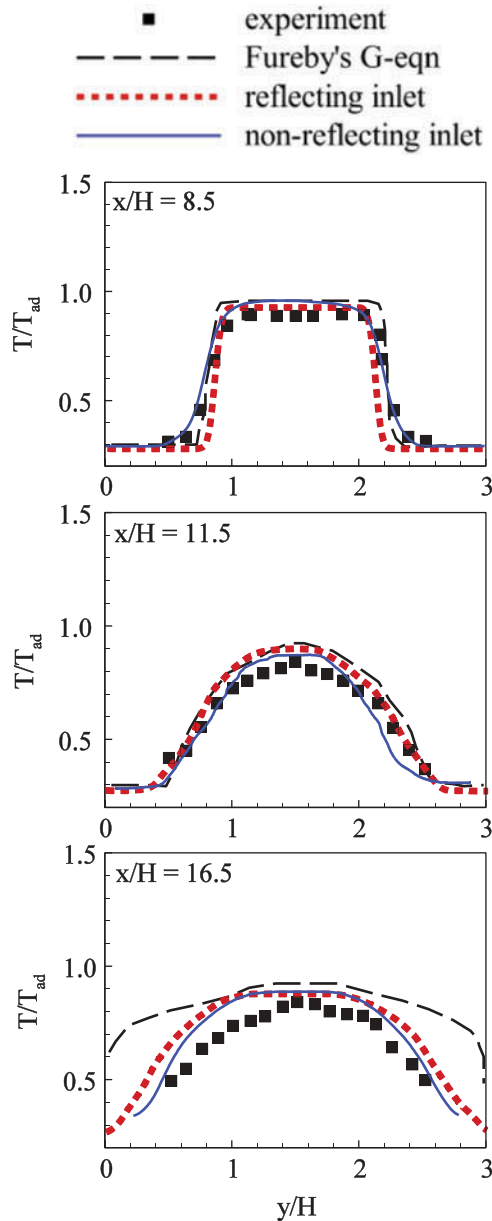


Figure 6. Vertical distributions of predicted and measured (Sjunnesson et al., 1991b) mean temperature at different streamwise locations ($x/H = 8.5, 11.5, 16.5$) for reacting flow.

in Baudoin et al. (2009). This can be attributed to the higher grid resolution and the non-reflective boundary condition that is used at the inlet in the current study. The inlet conditions with the acoustically non-reflecting boundary lead to the best overall match with the measurements, consistent with the fact that experimental conditions of Sjunnesson et al. (1991) more closely represent an acoustically non-reflecting inlet.

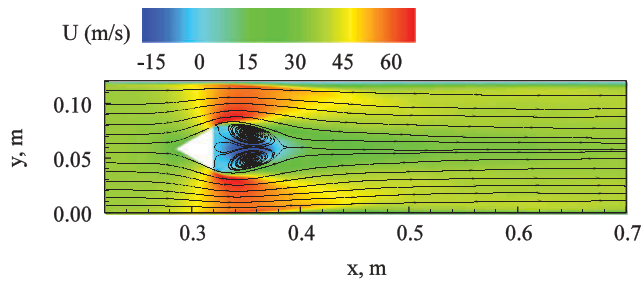


Figure 7. Time-mean distribution of axial velocity and streamlines at the mid-section in the spanwise direction for non-reacting flow.

Figure 7 shows the time-mean axial velocity field and streamlines at the mid-span section in the spanwise direction for the non-reacting case. The flowfield remains nearly two-dimensional, in spite of the 3D configuration. The flow accelerates in the bluff-body region due to the blockage effect. The shear layers originating from the edges of the bluff body and the recirculating flow behind the bluff body, as well as the wake, are clearly observed.

Figure 8 shows the time-mean distributions of the axial velocity and temperature, along with the streamlines, in the reacting flow. Both acoustically reflecting and non-reflecting inlet conditions are considered. The recirculation zone acts as a flame stabilization region, where hot products mix continuously with the incoming fuel/air mixture. Its behavior is mainly determined by the two separated shear layers. The volume dilatation and baroclinic effects caused by combustion reduce the intensity of the shear layers and inhibit their merger; thus, the recirculation zone is longer than that in the non-reacting flow. The flame spreading angle increases at the end of the recirculation zone. This phenomenon can be attributed to the flow acceleration and ensuing increase of turbulence intensity; flow expansion in the transverse direction also plays a contributing role. The case with an acoustically reflecting inlet shows a broader flame brush near the rear edges of the v-gutter.

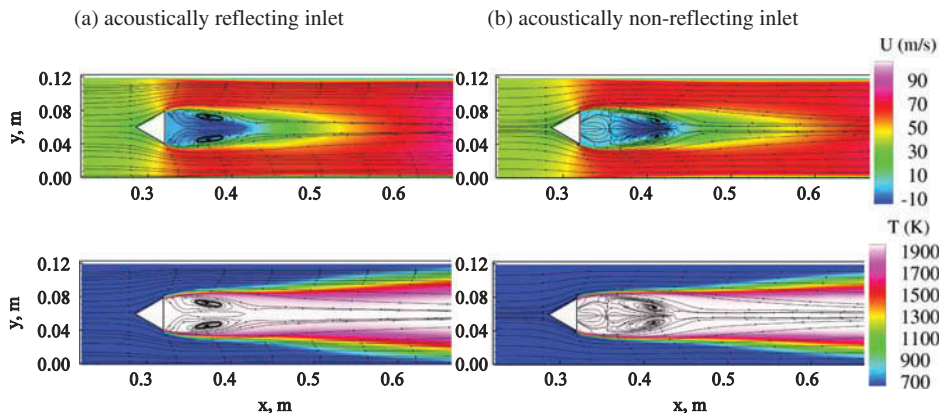


Figure 8. Time-mean distributions of axial velocity, streamline, and temperature at the mid-section in the spanwise direction for reacting flow: (a) acoustically reflecting inlet and (b) acoustically non-reflecting inlet.

Instantaneous flowfield

Figures 9–11 show instantaneous vorticity fields and flame fronts (defined by the isothermal surface of $T = 1300$ K). Both the acoustically reflecting and non-reflecting inlet cases are presented for comparison. The evolution of the vorticity fields and shear layers, as captured in Figure 9, is of great concern because of their dominant influence in determining the flow entrainment in the reaction zone and the subsequent flame evolution. In non-reacting flows, the sinuous wake downstream of the bluff body consists of separated shear layers and asymmetric vortex shedding (Cimbala, 1984). The behavior of the shear layer is primarily dictated by the Kelvin–Helmholtz instability, whereas the vortex shedding is determined by the BVK instability. In reacting flows, however, the BVK instability is suppressed by the exothermicity and volume dilatation in the flame zone. These effects, combined with baroclinicity, compete with viscous and turbulent diffusion and suppress the formation of BVK vortices. As a result, the BVK vorticity level is much lower in the reacting case than in its non-reacting counterpart. The near-field vorticity and flame-front distribution in Figure 11 clearly shows that the BVK vortex shedding is

acoustically reflecting inlet

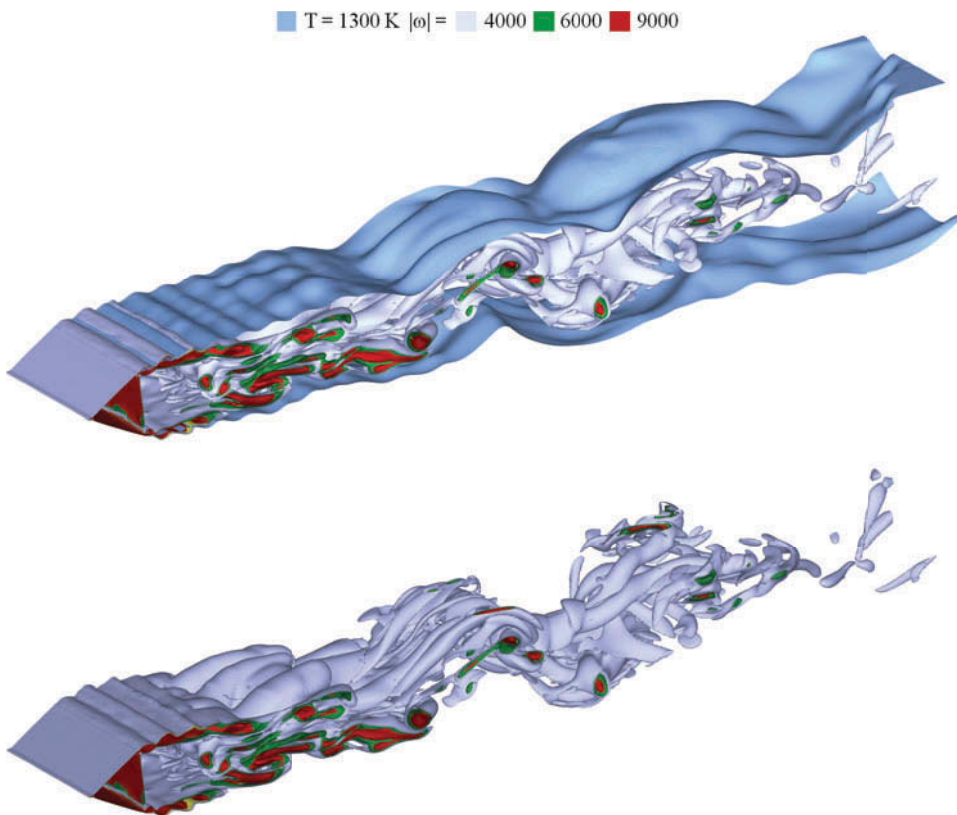


Figure 9a. Instantaneous flame front ($T = 1300$ K) (top) and vorticity field (bottom) in reacting flow for acoustically reflecting inlet.

acoustically non-reflecting inlet

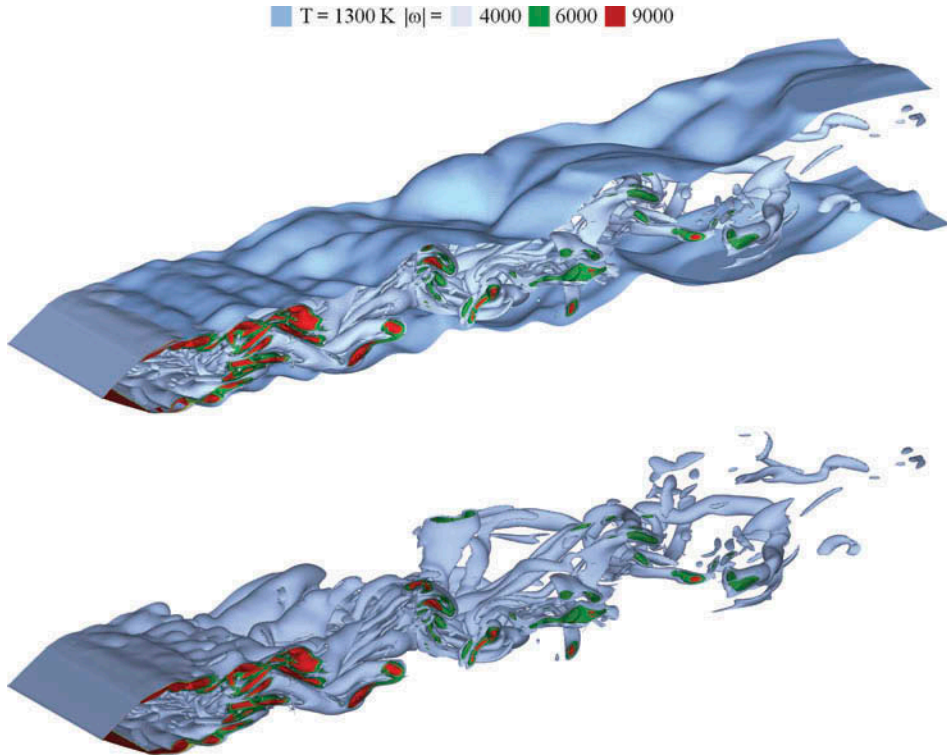


Figure 9b. Instantaneous flame front ($T = 1300\text{ K}$) (top) and vorticity field (bottom) in reacting flow for non-reflecting inlet.

constrained by heat release. A pair of symmetrical vortices appears at the opposite edges of the triangular bluff body, in contrast to the asymmetrical pattern of vortex shedding in the non-reacting flows. This result agrees with observations presented in previous numerical studies (Fureby, 2000; Giacomazzi et al., 2004).

The boundary layer around the bluff body adheres to the wall, since the Reynolds number is not very high. The shear layer then separates as it passes the trailing edges of the bluff body, and combined with the ensuing wake, governs the dynamics of the downstream flowfield. The separated shear layer leads to a longer recirculation zone and a weaker sinuous wake than in the corresponding non-reacting case. Figure 9b shows that the flame front is more stable for the case with the non-reflecting inlet than the reflecting one. Similarly, it can be observed from Figures 10b and 11b that the flame and the wake are more stable for the non-reflecting case. For both non-reacting and reacting flows, the separated shear layer is quasi two-dimensional in the spanwise direction, while the vortex shedding in the downstream region is highly three-dimensional. A 2D treatment, with a short spanwise computational domain, can usually obtain good agreement with experimental measurements in the near field (Giacomazzi et al., 2004). To achieve reliable predictions in the far field, however, a 3D analysis is essential.

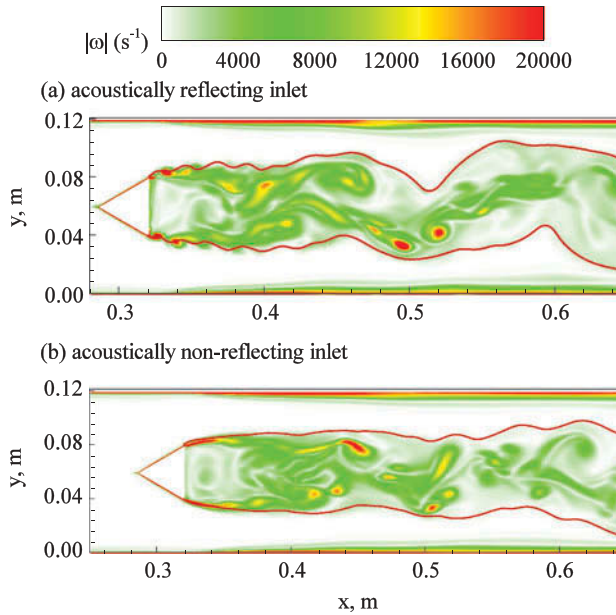


Figure 10. Instantaneous vorticity field (contour) and flame front of $T = 1300$ K (line).

When an acoustically reflecting inlet is enforced, an alternate vortex shedding pattern is observed; the frequency correlates well with the first transverse acoustic mode (see Figure 10a). In this mode the flame front wrinkles significantly, as illustrated in a close-up view of the near-field flow features in Figure 11a. In contrast, when an acoustically non-reflecting inlet is imposed, the shear layers at the opposite ends of the v -gutter are symmetric and the flame front is unwavering, as shown in Figures 10b and 11b. The acoustically non-reflecting inlet appears to be a reasonable representation of the experimental condition.

Flow dynamics and acoustic interaction

Since the most prominent type of instability in reacting flows involves the coupling between acoustic motion and transient combustion response, a prerequisite of any combustion instability research is the identification of acoustic modes in the chamber. An array of point probes were employed in the present study to record and characterize the flow evolution. Figures 12–14 show the frequency contents of the velocity and pressure fluctuations along the x -axis at three different vertical positions (near the top wall, in the shear layer, at the center line). Two dominant modes at frequencies of 236 Hz and 2480 Hz are observed.

To help provide physical insight, data analysis based on the proper-orthogonal-decomposition (POD) technique was performed to characterize the pressure field (Huang et al., 2006). Figure 15 shows the spatial distributions of the normal 1L (first longitudinal) and 1T/2L (mixed first transverse and second longitudinal) modes of pressure fluctuations. The instantaneous field of the pressure oscillation obtained from the LES study is also included for comparison. The dominant frequencies of the two modes are 240 Hz (1L)

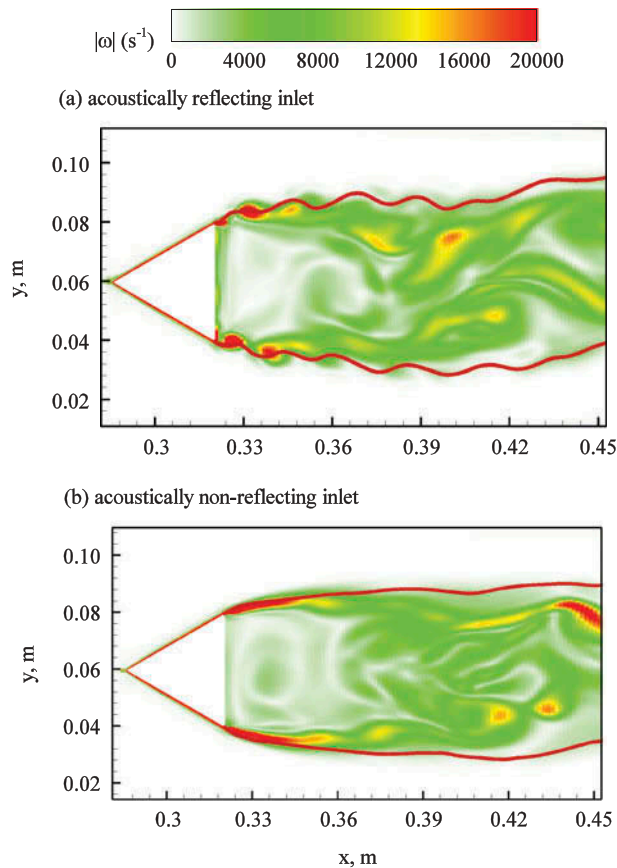


Figure 11. Close-up view of instantaneous vorticity field (contour) and flame front of $T = 1300$ K (line).

and 2430 Hz ($1T/2L$), respectively. Excellent agreement is achieved with the frequencies determined from the spectral analysis of the pressure data (see Figures 12–14). The non-symmetric distribution of the instantaneous pressure field arises from the flow and temperature non-uniformities in the chamber, as well as the geometric blockage imposed by the bluff body.

The inherent hydrodynamic instabilities of the separated shear layers and vortex shedding play a decisive role in determining the combustion dynamics of the chamber. When the characteristic frequencies of these processes match the chamber acoustic waves and heat-release response, intensive interactions occur and give rise to highly unsteady flow motions. The frequency spectra of pressure oscillations in Figures 12–14 indicate the dominance of the $1T/2L$ acoustic mode with its peak amplitude at the inlet wall (point 1 in Figure 12). The spectra of velocity oscillations show two dominant frequencies of flow motions. The lower one (310 Hz) corresponds to the BVK-related oscillation, and the higher one (2450 Hz) is associated with the shear layer instability. The resonance between the vortex shedding and acoustic motions leads to excitation of the $1T/2L$ acoustic mode in the chamber. It should be noted that, in addition to frequency matching, the spatial structure of the perturbation fields should be considered in the analysis.

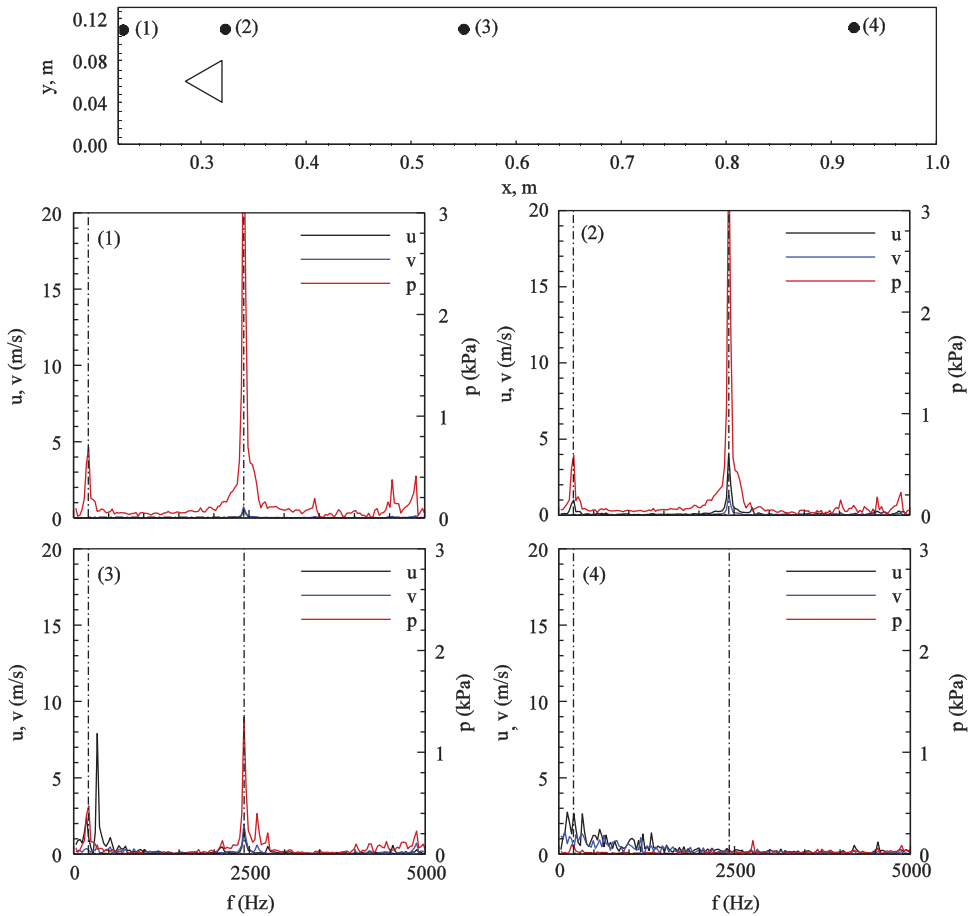


Figure 12. Power spectral densities of streamwise and transverse velocity components and pressure at positions near the top wall.

Unsteady flame evolution and vorticity coupling

The dynamics of the flame can be elucidated by considering its interaction with the local oscillatory flow. The entire process is dictated by the entrainment of fresh reactants and mixing with hot gases in the vortical regions in the flame zone. The instantaneous flame structures shown in Figure 16, along with their time-mean counterparts in Figure 8, clearly indicate that the flame is anchored at the trailing edges of the triangular bluff body. The flame exhibits a quasi-2D structure near the bluff body, but develops 3D structures in the downstream region. In the case with an acoustically reflecting inlet, the flame front shows a sinuous shape (see also Figure 10), compared to the relatively flat configuration for the case with a non-reflecting inlet.

Figure 17 shows the instantaneous vorticity fields for all the cases considered. The near-field flame evolution is influenced mainly by the quasi 2D separated shear layers, while in the far field the flame is dominated by the large 3D vortical structures. Figure 17b indicates that vortex roll-up takes place immediately downstream of the bluff-body trailing

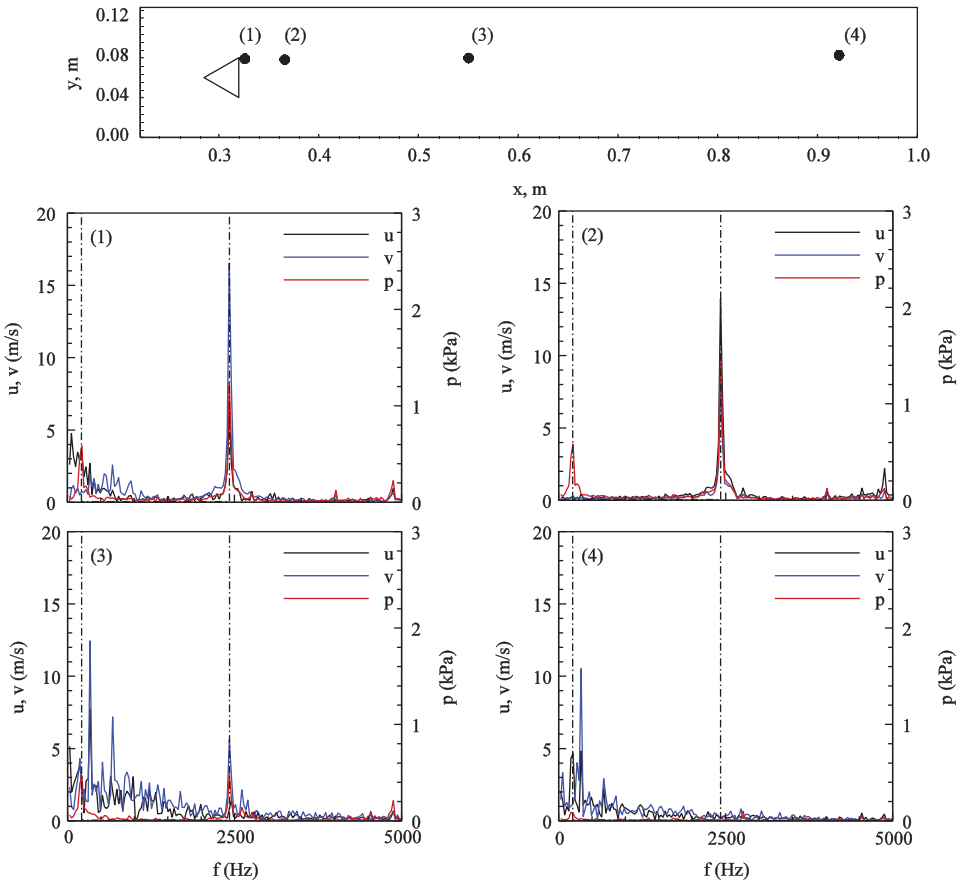


Figure 13. Power spectral densities of streamwise and transverse velocity components and pressure at positions along $y = 0.08$ m.

edge; this is a consequence of the coupling between acoustic waves and shear-layer instabilities. The vortices distort the flame, which is anchored at the edges, and this gives rise to a sinuous flame front. For the non-reflecting inlet boundary, on the other hand, two relatively flat separated shear layers originate from the trailing edges. The flame is embedded in the shear layer, and no sinuous distortion of the flame front is exhibited in the near field.

Figure 18 shows the temporal evolution of the vorticity field and the flame front over one cycle of the $1T/2L$ mode of acoustic oscillation for the case with an acoustically reflecting inlet. The phase angle θ is referenced with respect to the acoustic pressure at the upper trailing edge. During the pressure build-up stage ($\theta = 0-180^\circ$), a vortex is shed from the upper trailing edge, inducing a positive (upward) transverse velocity at that location. The increasing pressure and associated favorable gradient facilitate entrainment of fresh reactants into the flame zone. Heat release intensifies and sustains acoustic excitation through the energy transfer. The resultant flow expansion tends to push the anchored flame vertically outward. During the pressure-drop stage of the cycle ($\theta = 180-360^\circ$), a new vortex forms at the upper trailing edge, inducing negative (downward) transverse velocity. The decreasing pressure and associated adverse

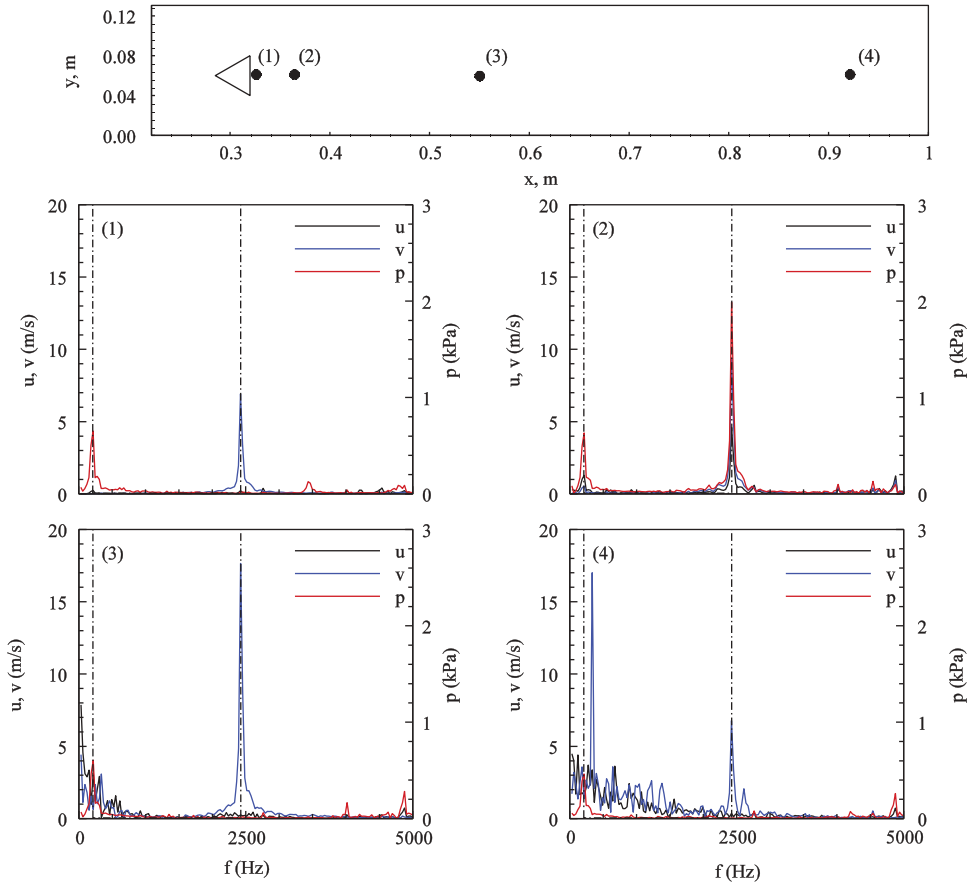


Figure 14. Power spectral densities of streamwise and transverse velocity components and pressure at positions along the centerline of the chamber.

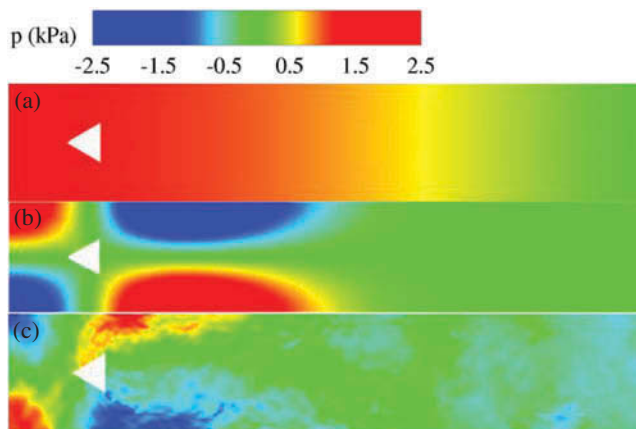
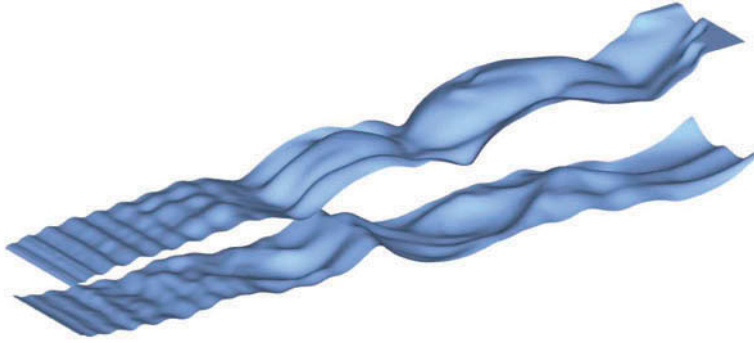


Figure 15. Spatial distributions of pressure oscillation: (a) 1L and (b) 1T/2L POD acoustic mode, and (c) instantaneous field predicted by LES.

(a) acoustically reflecting inlet



(b) acoustically non-reflecting inlet

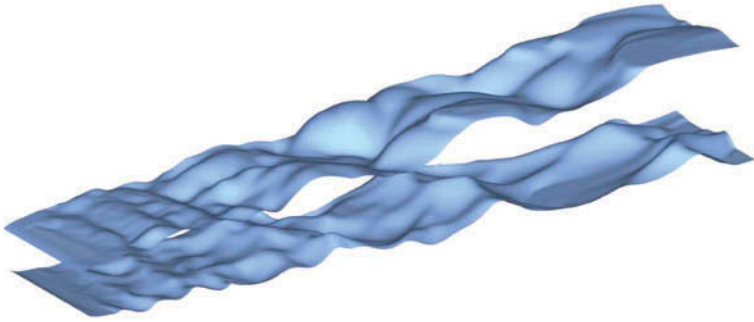


Figure 16. Spatial evolution of flame front ($T = 1300$ K): (a) acoustically reflecting inlet and (b) acoustically non-reflecting inlet.

gradient prevent entrainment of fresh reactants into the flame zone, thus decreasing the local heat release. The anchored flame is pushed inwards toward the chamber centerline. Comparison of the first and second rows in Figure 18 indicates a phase difference of 180° between the shed vortices. Also shown are the out-of-phase oscillations of the flame fronts anchored at the upper and lower trailing edges. The corresponding acoustic waves in the transverse direction at those two locations exhibit 180° phase difference, consistent with the $1T/2L$ acoustic mode obtained from the POD analysis. These phenomena indicate strong interactions among vortex shedding, flame oscillations, and acoustic motion in the chamber.

Coupling between acoustic and heat-release oscillations

The mutual coupling between heat release and acoustic wave can be characterized using the Rayleigh parameter, $Ra(\mathbf{x})$, defined as the time-averaged product of the pressure oscillation $p'(\mathbf{x}, t)$ and heat-release fluctuation $q'(\mathbf{x}, t)$ (Huang et al., 2006; Rayleigh, 1945):

$$Ra(\mathbf{x}) = \frac{1}{\tau} \int_{\tau} p'(\mathbf{x}, t) q'(\mathbf{x}, t) dt \quad (18)$$

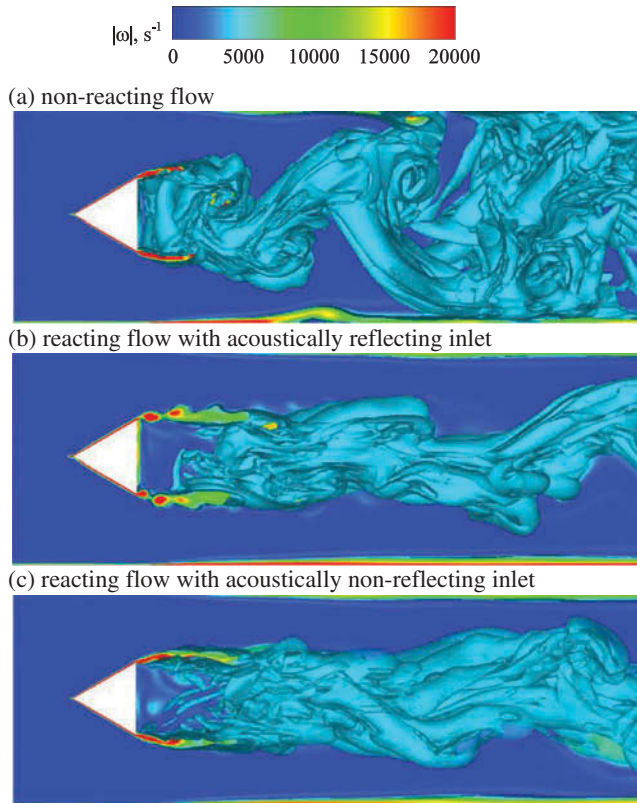


Figure 17. Instantaneous vorticity fields at the mid-section in the spanwise direction: (a) non-reacting flow, (b) reacting flow with reflecting inlet, and (c) reacting flow with non-reflecting inlet.

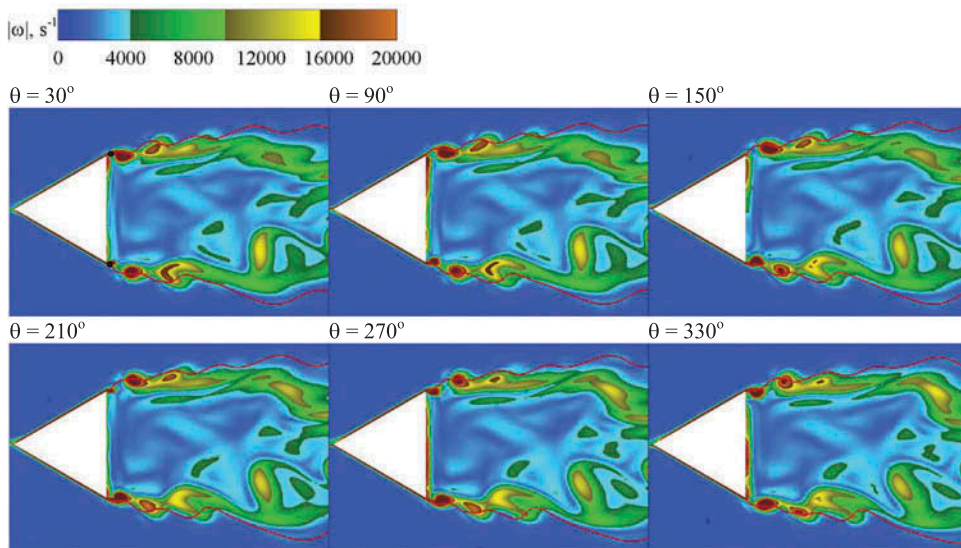


Figure 18. Temporal evolution of the vorticity field (color) and flame front (line) over one cycle of the $1T/2L$ mode of acoustic oscillation for an acoustically reflecting inlet.

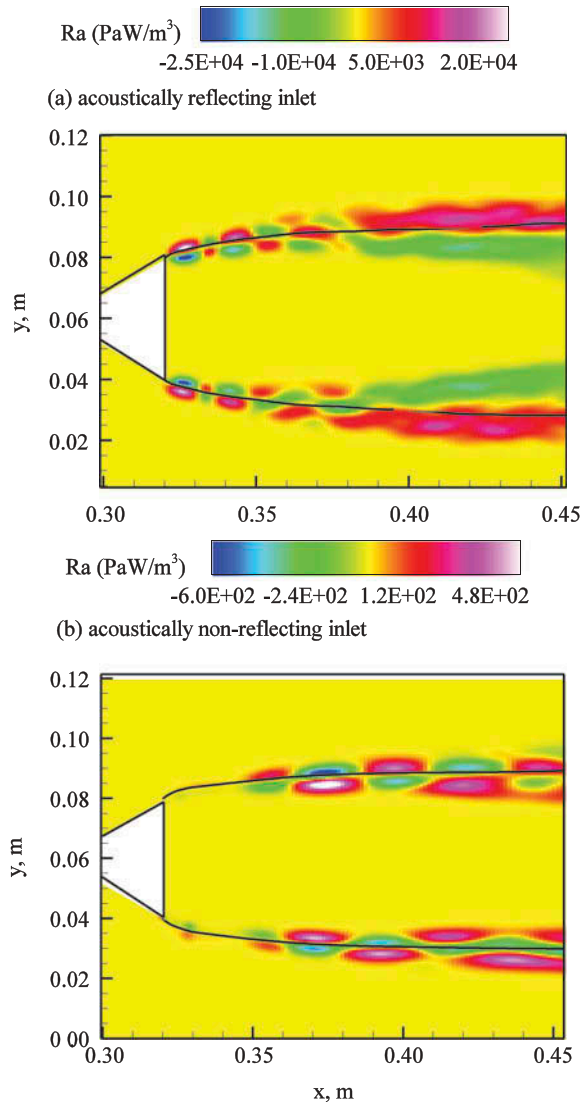


Figure 19. Distribution of Rayleigh parameter.

where τ is the time period of oscillation. The Rayleigh parameter provides a qualitative measure of the extent to which unsteady heat release drives or suppresses instabilities. The acoustic oscillation is amplified if $Ra(\mathbf{x}) > 0$, or damped if $Ra(\mathbf{x}) < 0$. Figure 19 presents the spatial distributions of the Rayleigh parameter and the mean flame position (denoted by line). An organized pattern is observed in the Rayleigh parameter; this suggests coupling between unsteady heat release and acoustic waves. The Rayleigh parameter is almost two orders of magnitude larger for the case with an acoustically reflecting inlet than for the non-reflecting counterpart, because of stronger pressure and heat-release oscillations and in-phase coupling between the two.

Figure 19a shows that for an acoustically reflecting inlet the Rayleigh parameter is generally positive on the unburned side of the flame front and negative on the burned

side. When the flame expands outward in the transverse direction, the pressure follows the heat release trend, rendering a positive correlation on the burned side and a negative trend on the unburned side. Acoustic waves extract energy from the oscillating heat release and continue to amplify over the exothermic part of the cycle. The maximum Rayleigh parameter appears along the separated shear layers in the near field of the bluff body. This observation is consistent with the strong coupling that is exhibited between separated shear layers and acoustic waves, as explained in the previous section.

For an acoustically non-reflecting inlet (Figure 19b), the Rayleigh parameter exhibits a pattern of staggered dipoles. Acoustic pressure rises and drops periodically along the flame, with a phase difference of 180° across the flame surface. This type of alternate distribution tends to balance out the overall pressure fluctuations, so the acoustic waves undergo less amplification than in the case of a reflecting inlet boundary, making the combustion process relatively stable.

The physiochemical processes in the chamber feature a wide range of oscillation frequencies. When the characteristic frequencies of these processes match those of the chamber acoustic waves, strong interactions occur and give rise to intensive excitations of flow oscillations. The resulting favorable coupling among acoustic waves, vortex shedding, and unsteady heat release forms a feedback loop causing severe combustion instabilities.

Conclusions

A comprehensive numerical analysis has been performed by means of an LES technique to investigate the dynamical behavior of a flame stabilized by a triangular bluff body in a straight chamber. Turbulence/chemistry interaction was treated using a G-equation-based level-set flamelet library model. The overall approach was validated against experimental measurements of the time-mean and turbulent velocities for both non-reacting and reacting flows. Good agreement was achieved between calculated and measured data.

Detailed flow evolution was explored systematically for both non-reacting and reacting cases. For reacting flows, the importance of employing appropriate acoustic boundary conditions was confirmed by comparing the results of cases with acoustically reflecting and non-reflecting inlets. For the former condition, the vortex shedding frequency of the shear layer separated from the bluff body matched closely with the 1L and 1T/2L acoustic modes of the chamber. The vortical motions in the flame zone resonate with the acoustic waves in the chamber, giving rise to large-amplitude flow oscillations. The flame dynamics are determined by the interactions between the separated shear layers and acoustic waves, driven by the fluctuating heat release in the flame zone. The resulting interplay among acoustic fluctuations, vortex shedding, and unsteady heat release forms a feedback loop causing severe combustion instabilities. An acoustically reflecting inlet, combined with a low density ratio, tends to lead to unfavorable flame dynamics. Future studies should be conducted to develop mitigation strategies for such configurations.

Acknowledgment

The support and encouragement provided by Dr. Mitat Birkan of the Air Force Office of Scientific Research (AFOSR) is gratefully acknowledged.

Funding

This work was sponsored partly by the AFOSR under contract no. FA9550-10-1-0179, and partly by the William R. T. Oakes Endowment of the Georgia Institute of Technology.

Nomenclature

a	=	speed of sound
CFL	=	Courant–Friedrichs–Lewy
E	=	specific total energy
f	=	frequency (Hz)
G	=	level-set variable
H	=	channel height
k	=	wave number
Ka	=	Karlovitz number
l_F	=	laminar flame thickness
l_δ	=	inner-layer flame thickness
\mathbf{n}	=	unit vector normal to flame front
p	=	pressure
q	=	rate of heat release per unit volume
R	=	gas constant
Re	=	Reynolds number
S_L	=	flame speed
t	=	time
T	=	temperature
T_b	=	temperature of burnt mixture
T_u	=	temperature of unburnt mixture
u_i	=	velocity

Greek symbols

ρ	=	density
τ_{ij}	=	shear stress tensor
λ	=	thermal conductivity
η	=	Kolmogorov length scale
φ	=	equivalence ratio
γ	=	ratio of specific heats
θ	=	phase angle
σ_i	=	viscous work

Superscripts

sgs	=	subgrid scale
–	=	ensemble averaging

- ~ = Favre averaging
 ' = fluctuation

Subscripts

- 0 = initial time
 a = acoustic
 in = inlet flow
 t = turbulent

References

- Apte, S.V., and Yang, V. 2003. A large-eddy simulation study of transition and flow instability in a porous-walled chamber with mass injection. *J. Fluid Mech.*, **477**, 215–225.
- Baudoin, E., Yu, R., Nogenmyr, K.J., Bai, X.S., and Fureby, C. 2009. Comparison of LES models applied to a bluff body stabilized flame. AIAA Paper 2009–1178.
- Briones, A.M., Sekar, B., and Thornburg, H. 2011. Characteristics of bluff body stabilized turbulent premixed flames. Presented at the ASME Turbo Expo: Turbine Technical Conference and Exposition, Vancouver, Canada, June 6–10.
- Cimbala, J.M. 1984. *Large Structure in the Far Wakes of Two-Dimensional Bluff Bodies*. California Institute of Technology, Pasadena, CA.
- Cocks, P.A.T., Soteriou, M.C., and Sankaran, V. 2015. Impact of numerics on the predictive capabilities of reacting flow LES. *Combust. Flame*, **162**, 3394–3411.
- Emerson, B., O'Connor, J., Juniper, M., and Lieuwen, T. 2012. Density ratio effects on reacting bluff-body flow field characteristics. *J. Fluid Mech.*, **706**, 219–250.
- Engdar, U., Nilsson, P., and Klingmann, J. 2003. Investigation of turbulence models applied to premixed combustion using a level-set flamelet library approach. Presented at the ASME Turbo Expo 2003 (collocated with the 2003 International Joint Power Generation Conference), Atlanta, GA, June 16–19.
- Engdar, U., Nilsson, P., and Klingmann, J. 2004. Investigation of turbulence models applied to premixed combustion using a level-set flamelet library approach. *J. Eng. Gas Turbines Power*, **126**, 701–707.
- Erickson, R.R., and Soteriou, M.C. 2011. The influence of reactant temperature on the dynamics of bluff body stabilized premixed flames. *Combust. Flame*, **158**, 2441–2457.
- Erickson, R.R., Soteriou, M.C., and Mehta, P.G. 2006. The influence of temperature ratio on the dynamics of bluff body stabilized flames. AIAA Paper 2006-753. Presented at the 44th AIAA Aerospace Sciences Meeting and Exhibit, Reno, NV, January 9–12.
- Erlebacher, G., Hussaini, M.Y., Speziale, C.G., and Zang, T.A. 1992. Toward the large-eddy simulation of compressible turbulent flows. *J. Fluid Mech.*, **238**, 155–185.
- Fujii, S., and Eguchi, K. 1981. A comparison of cold and reacting flows around a bluff-body flame stabilizer. *J. Fluids Eng.*, **103**, 328–334.
- Fung, Y.-T., and Yang, V. 1992. Active control of nonlinear pressure oscillations in combustion chambers. *J. Propul. Power*, **8**, 1282–1289.
- Fung, Y.-T., Yang, V., and Sinha, A. 1991. Active control of combustion instabilities with distributed actuators. *Combust. Sci. Technol.*, **78**, 217–245.
- Fureby, C. 1996. On subgrid scale modeling in large eddy simulations of compressible fluid flow. *Phys. Fluids*, **8**, 1301–1311.
- Fureby, C. 2000. A computational study of combustion instabilities due to vortex shedding. *Proc. Combust. Inst.*, **28**, 783–791.
- Fureby, C. 2006. A comparison of flamelet les models for premixed turbulent combustion. AIAA Paper 2006–155.

- Fureby, C. 2007a. Comparison of flamelet and finite rate chemistry models for premixed turbulent combustion. *AIAA Paper* 2007-1413.
- Fureby, C. 2007b. ILES and LES of complex engineering turbulent flows. *J. Fluids Eng.*, **129**, 1514-1523.
- Fureby, C., and Löfström, C. 1994. Large-eddy simulations of bluff body stabilized flames. *Symp. (Int.) Combust.*, **25**, 1257-1264.
- Fureby, C., and Möller, S.-I. 1995. Large eddy simulation of reacting flows applied to bluff body stabilized flames. *AIAA J.*, **33**, 2339-2347.
- Ge, H.-W., Zhu, M.-M., Chen, Y.-L., and Gutheil, E. 2007. Hybrid unsteady RANS and PDF method for turbulent non-reactive and reactive flows. *Flow Turbul. Combust.*, **78**, 91-109.
- Ghirelli, F. 2011. Turbulent premixed flame model based on a recent dispersion model. *Comput. Fluids*, **44**, 369-376.
- Giacomazzi, E., Battaglia, V., and Bruno, C. 2004. The coupling of turbulence and chemistry in a premixed bluff-body flame as studied by LES. *Combust. Flame*, **138**, 320-335.
- Grinstein, F.F., Rider, W.J., and Margolin, L.G. 2007. *Implicit Large Eddy Simulation*, Cambridge University Press, Cambridge, UK.
- Herrmann, M. 2000. Numerical simulation of premixed turbulent combustion based on a level set flamelet model. PhD thesis. der Rheinisch-Westfälischen Technischen Hochschule Aachen University, Aachen, Germany.
- Huang, Y., Sung, H.-G., Hsieh, S.-Y., and Yang, V. 2003. Large-eddy simulation of combustion dynamics of lean-premixed swirl-stabilized combustor. *J. Propul. Power*, **19**, 782-794.
- Huang, Y., Wang, S., and Yang, V. 2006. Systematic analysis of lean-premixed swirl-stabilized combustion. *AIAA J.*, **44**, 724-740.
- Jones, W.P., Marquis, A.J., and Wang, F. 2015. Large eddy simulation of a premixed propane turbulent bluff body flame using the Eulerian stochastic field method. *Fuel*, **140**, 514-525.
- Kim, J., and Pope, S.B. 2014. Effects of combined dimension reduction and tabulation on the simulations of a turbulent premixed flame using a large-eddy simulation/probability density function method. *Combust. Theory Modell.*, **18**, 388-413.
- Lee, C., and Cant, R. 2014. CFD investigation of hydrodynamic and acoustic instabilities of bluff-body stabilized turbulent premixed flames. Presented at the ASME Turbo Expo: Turbine Technical Conference and Exposition, Dusseldorf, Germany, June 16-20.
- Lieuwen, T.C., and Yang, V. (Eds.). 2005. *Combustion Instabilities in Gas Turbine Engines: Operational Experience, Fundamental Mechanisms and Modeling*, American Institute of Aeronautics and Astronautics, Reston, VA.
- Lieuwen, T.C., and Yang, V. (Eds.). 2013. *Gas Turbine Emissions*, Cambridge University Press, Cambridge, UK.
- Lin, C.-X., and Holder, R.J. 2010. Reacting turbulent flow and thermal field in a channel with inclined bluff body flame holders. *J. Heat Transfer*, **132**, 091203.
- Manickam, B., Franke, J., Muppala, S.R., and Dinkelacker, F. 2012. Large-eddy simulation of triangular-stabilized lean premixed turbulent flames: Quality and error assessment. *Flow Turbul. Combust.*, **88**, 563-596.
- Marble, F.E., and Candel, S.M. 1979. An analytical study of the non-steady behavior of large combustors. *Proc. Combust. Inst.*, **17**, 761-769.
- Moreau, V. 2009. A self-similar premixed turbulent flame model. *Appl. Math. Modell.*, **33**, 835-851.
- Nilsson, P., and Bai, X.S. 2000. Level-set flamelet library approach for premixed turbulent combustion. *Exp. Therm. Fluid Sci.*, **21**, 87-98.
- Oefelein, J.C., and Yang, V. 1996. Simulation of high-pressure spray field dynamics. recent advances in spray combustion: Spray combustion measurements and model simulation. *Prog. Astronaut. Aeronaut.*, **171**, 263-304.
- Olovsson, S. 1992. Combustion calculations on a premixed system with a bluff body flameholder. Presented at the 28th Joint Propulsion Conference and Exhibit, Nashville, TN, July 6-8.
- Park, N., and Ko, S. 2011. Large eddy simulation of turbulent premixed combustion flow around bluff body. *J. Mech. Sci. Technol.*, **25**, 2227-2235.
- Peters, N. 2000. *Turbulent Combustion*, Cambridge University Press, Cambridge, UK.

- Poinsot, T., and Veynante, D. 2005. *Theoretical and Numerical Combustion*, R.T. Edwards Inc., Flourtown, PA.
- Porumbel, I., and Menon, S. 2006. Large eddy simulation of bluff body stabilized premixed flame. Presented at the 44th AIAA Aerospace Sciences Meeting and Exhibit, Reno, NV, January 9–12.
- Prasad, A., and Williamson, C.H.K. 1997. The instability of the shear layer separating from a bluff body. *J. Fluid Mech.*, **333**, 375–402.
- Rayleigh, J.W.S.B. 1945. *The Theory of Sound*, Dover, New York.
- Ryden, R., Eriksson, L.-E., and Olovsson, S. 1993. Large eddy simulation of bluff body stabilised turbulent premixed flames. Presented at the ASME 1993 International Gas Turbine and Aeroengine Congress and Exposition, Cincinnati, OH, May 24–27.
- Sagaut, P. 2002. *Large Eddy Simulation for Incompressible Flows*, Springer, Leipzig, Germany.
- Salvador, N.M.C., de Mendonça, M.T., and da Costa Dourado, W.M. 2013. Large eddy simulation of bluff body stabilized turbulent premixed flame. *J. Aerosp. Technol. Manage.*, **5**, 181–196.
- Sanquer, S., Bruel, P., and Deshaies, B. 1998. Some specific characteristics of turbulence in the reactive wakes of bluff bodies. *AIAA J.*, **36**, 994–1001.
- Shanbhogue, S.J., Husain, S., and Lieuwen, T. 2009a. Lean blowoff of bluff body stabilized flames: scaling and dynamics. *Prog. Energy Combust. Sci.*, **35**, 98–120.
- Shanbhogue, S.J., Plaks, D.V., and Lieuwen, T. 2007. The K-H instability of reacting, acoustically excited bluff-body shear layers. AIAA Paper 2007–5860.
- Shanbhogue, S.J., Shin, D.-H., Hemchandra, S., Plaks, D., and Lieuwen, T. 2009b. Flame-sheet dynamics of bluff-body stabilized flames during longitudinal acoustic forcing. *Proc. Combust. Inst.*, **32**, 1787–1794.
- Shcherbik, D., Cross, C.N., Fricker, A., Bibik, O., Scarborough, D., Lubarsky, E., and Zinn, B.T. 2009. Dynamics of v-gutter-stabilized jet-a flames in a single flame holder combustor with full optical access. AIAA Paper 2009–5291.
- Shin, D.-H., Plaks, D.V., Lieuwen, T., Mondragon, U.M., Brown, C.T., and McDonell, V.G. 2011. Dynamics of a longitudinally forced, bluff body stabilized flame. *J. Propul. Power*, **27**, 105–116.
- Sivakumar, R., and Babu, V. 2008. Numerical simulations of the 3D unsteady flow in a bluff-body combustor. *Int. J. Aeroacoust.*, **7**, 301–320.
- Sivakumar, R., and Chakravarthy, S.R. 2008. Experimental investigation of the acoustic field in a bluff-body combustor. *Int. J. Aeroacoust.*, **7**, 267–299.
- Sjunnesson, A., Henrikson, P., and Lofstrom, C. 1992. Cars measurements and visualization of reacting flows in a bluff body stabilized flame. Presented at the 28th Joint Propulsion Conference and Exhibit, Nashville, TN, July 6–8.
- Sjunnesson, A., Olovsson, S., and Sjöblom, B. 1991a. Validation rig—A tool for flame studies. Presented at the 10th International Symposium on Air Breathing Engines, Nottingham, England, September 1–6.
- Sjunnesson, A., Olovsson, S., and Sjöblom, B. 1991b. Validation rig—A tool for flame studies. Volvo Flygmotor Internal Report VFA 9370–308.
- Sundaram, S.S., and Babu, V. 2013. Numerical investigation of combustion instability in a v-gutter stabilized combustor. *J. Eng. Gas Turbines Power*, **135**, 121501.
- Sussman, M., Smerka, P., and Osher, S. 1994. A level set approach for computing solutions to incompressible two-phase flow. *J. Comput. Phys.*, **114**, 146–159.
- Tsien, H.S. 1951. Influence of flame front on the flow field. *J. Appl. Mech.*, **18**, 188–194.
- Wang, S., and Yang, V. 2005. Unsteady flow evolution in swirl injectors with radial entry. II. External excitations. *Phys. Fluids*, **17**, 045107.
- Wang, S., Yang, V., Hsiao, G., Hsieh, S.-Y., and Mongia, H.C. 2007. Large-eddy simulations of gas-turbine swirl injector flow dynamics. *J. Fluid Mech.*, **583**, 99–122.
- Yang, V., and Culick, F.E.C. 1986. Analysis of low frequency combustion instabilities in a laboratory ramjet combustor. *Combust. Sci. Technol.*, **45**, 1–25.
- Zhou, L.X., Hu, L.Y., and Wang, F. 2008. Large-eddy simulation of turbulent combustion using different combustion models. *Fuel*, **87**, 3123–3131.

- Zukoski, E.E. 1997. Afterburners. In G. Oates (Ed.), *Aerothermodynamics of Gas Turbine and Rocket Propulsion*, American Institute of Aeronautics and Astronautics, Reston, VA, pp. 47–147.
- Zukoski, E.E., and Marble, F.E. 1956. Experiments concerning the mechanism of flame blowoff from bluff bodies. In *Proceedings of the Gas Dynamics Symposium on Thermochemistry*, p. Northwestern University Press, Evanston, IL, p. 205.